

# Enhanced Hydrogen Production from DNA-Assembled Z-Scheme $\text{TiO}_2$ -CdS Photocatalyst Systems\*\*

Ke Ma, Omer Yehezkeili, Dylan W. Domaille, Hans H. Funke, and Jennifer N. Cha\*

**Abstract:** A wide range of inorganic nanostructures have been used as photocatalysts for generating  $\text{H}_2$ . To increase activity, Z-scheme photocatalytic systems have been implemented that use multiple types of photoactive materials and electron mediators. Optimal catalysis has previously been obtained by interfacing different materials through aggregation or epitaxial nucleation, all of which lowers the accessible active surface area. DNA has now been used as a structure-directing agent to organize  $\text{TiO}_2$  and CdS nanocrystals. A significant increase in  $\text{H}_2$  production compared to CdS or  $\text{TiO}_2$  alone was thus observed directly in solution with no sacrificial donors or applied bias. The inclusion of benzoquinone (BQ) equidistant between the  $\text{TiO}_2$  and CdS through DNA assembly further increased  $\text{H}_2$  production. While the use of a second quinone in conjunction with BQ showed no more improvement, its location within the Z-scheme was found to strongly influence catalysis.

With increasing demands for alternative sources of fuel, extensive research has focused on discovering methods to generate renewable energy from earth-abundant resources. In recent years, a wide range of inorganic nanostructures with high surface areas and tunable band gaps have been synthesized and used as photocatalysts for splitting water into hydrogen and oxygen.<sup>[1–23]</sup> To increase their activity, Z-scheme photocatalytic systems have been implemented in which multiple types of photoactive materials simultaneously oxidize water and reduce molecules upon photoillumination.<sup>[1–12]</sup> In some cases, redox molecules or electron mediators have also been used to aid in electron shuttling between the different catalysts, facilitate charge separation, and inhibit recombination events. For example, Sasaki et al. recently showed that by mixing  $\text{Ru}/\text{SrTiO}_3:\text{Rh}$  with  $\text{BiVO}_4$  and inducing aggregation through pH changes that higher

amounts of  $\text{H}_2$  and  $\text{O}_2$  could be produced than either material alone.<sup>[1]</sup> In later work, they showed that adding  $[\text{Co}(\text{bpy})_3]^{2+}/[\text{Co}(\text{bpy})_3]^{3+}$  as redox mediators further enhanced water splitting performance.<sup>[2]</sup> Abe et al. reported similar work in which  $\text{IO}_3^-/\text{I}^-$  was utilized to shuttle electrons between  $\text{TiO}_2$  rutile and Pt-loaded  $\text{TiO}_2$  anatase to produce  $\text{H}_2$  under UV light.<sup>[3]</sup> To achieve catalysis under visible light, Kato and co-workers used a  $\text{Pt}/\text{SrTiO}_3:\text{Rh}-\text{BiVO}_4$  system with  $\text{Fe}^{3+}/\text{Fe}^{2+}$  as redox mediators.<sup>[4]</sup> Recently, solid-state Z-scheme systems have also been synthesized in which control over the interface between the different materials was found to be critical for higher fuel production.<sup>[5,17–22]</sup> For example, Tada et al. developed an anisotropic CdS/Au/ $\text{TiO}_2$  system in which all the components were spatially fixed with Au facilitating electron transfer.<sup>[5]</sup> Metals other than gold have also been tested, including Ag,<sup>[20]</sup> Cd,<sup>[18]</sup> Cu,<sup>[19]</sup> ITO,<sup>[20]</sup> and reduced graphene oxide.<sup>[21]</sup>

In almost all of these cases, optimal catalysis is typically obtained by interfacing different materials through aggregation (for example, electrostatic interactions<sup>[1]</sup>) or epitaxial nucleation of one material on top of another. These methods, however, tend to decrease the overall accessible catalytic surface area because of the limited control over spatial organization of the separate components. Furthermore, the scope of different materials that can be produced by direct chemical synthesis is limited. Finally, since electron transfer largely depends on diffusion, simply mixing electron mediators with different catalysts in solution requires a high concentration of redox molecules to avoid rate limitations but which can lead to undesired side oxidation/reduction reactions. To address these challenges, we utilize DNA in this work as a structure-directing agent<sup>[23–36]</sup> to spatially organize well-defined  $\text{TiO}_2$  and Pt decorated CdS (Pt@CdS) nanocrystals. By using DNA as an assembler, a significant increase in  $\text{H}_2$  production was observed upon photoillumination compared to Pt@CdS or  $\text{TiO}_2$  alone directly in solution. Potential limitations in  $\text{H}_2$  production caused by negatively charged DNA on the Pt@CdS nanoparticles was simply fixed by controlling the amount of DNA per CdS nanorod. DNA also allowed positioning of a single or series of electron mediators site-specifically in between the two catalysts.

Well-defined Pt decorated CdS nanorods (NRs) and  $\text{TiO}_2$  nanoparticles (NPs) were implemented as photocatalysts for the DNA-linked Z-scheme. Based on their respective energy levels, CdS or Pt@CdS should be able to efficiently reduce  $\text{H}^+$  to  $\text{H}_2$  but  $\text{TiO}_2$  cannot.  $\text{TiO}_2$  NPs and CdS NRs were synthesized according to previous reports.<sup>[37,38]</sup> As shown in Figure 1a, the as-synthesized  $\text{TiO}_2$  NPs possessed truncated rhombic shapes that were approximately 25 nm in length and 15 nm in diameter. The X-ray diffraction (XRD) analysis of

[\*] K. Ma, Dr. O. Yehezkeili, Prof. D. W. Domaille, Prof. H. H. Funke, Prof. J. N. Cha  
Department of Chemical and Biological Engineering  
University of Colorado, Boulder, CO 80309-0596 (USA)  
E-mail: Jennifer.Cha@colorado.edu

Prof. J. N. Cha  
Materials Science and Engineering Program  
University of Colorado (USA)

[\*\*] The research was primarily supported by the U.S. Dept of Energy (DOE), Office of Science, Basic Energy Sciences (BES) under Award DE-SC0006398 (synthesis, assembly). In addition the research was supported by the Office of Naval Research under Award N00014-09-01-0258 (synthesis, microscopy characterization, catalytic studies). O.Y. was supported by DOE DE-SC0006398.

Supporting information for this article is available on the WWW under <http://dx.doi.org/10.1002/anie.201504155>.

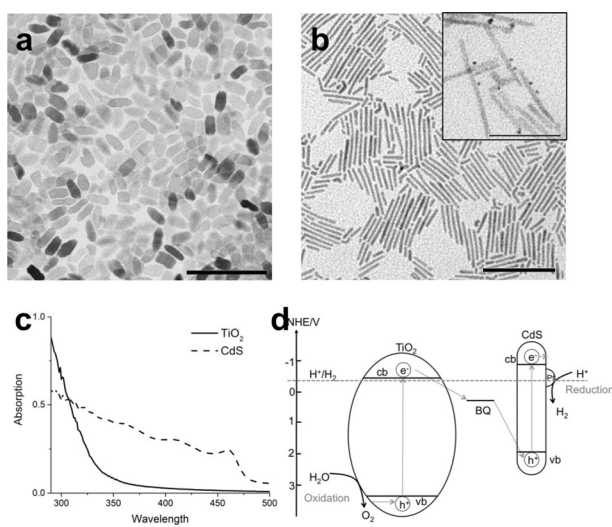


**Figure 1.** a) TEM image of  $\text{TiO}_2$  nanocrystals with truncated rhombic shape. b) TEM image of CdS nanorods. Insert: Pt decorated CdS nanorods. c) UV/Vis spectrum of as-synthesized CdS nanorods and  $\text{TiO}_2$  nanocrystals. d) Energy band diagram of the CdS-benzoquinone- $\text{TiO}_2$  system at pH 7. BQ = benzoquinone, cb = conduction band, vb = valence band. Scale bar: 100 nm.

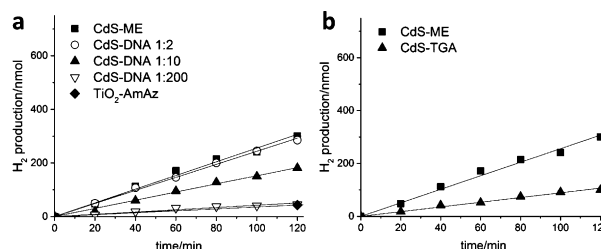
the  $\text{TiO}_2$  particles (Supporting Information, Figure S1) showed them to have an anatase structure, and the UV/Vis measurements showed a strong absorption at about 350 nm (Figure 1c). As shown in Figure 1b, the CdS nanorods were about 6 nm in width and average 60 nm in length, which corresponded to an absorption onset of about 490 nm. Since the bandgap of the synthesized CdS NRs is about 2.7 eV, the rods should absorb all photon wavelengths less than 490 nm, while the  $\text{TiO}_2$  bandgap of 3.83 eV causes it to absorb primarily in the UV range. The valence band and conduction band of the  $\text{TiO}_2$  NPs were investigated by cyclic voltammetry (CV; Supporting Information, Figure S2).<sup>[39]</sup> As shown in Figure 1d, the conduction band of the  $\text{TiO}_2$  NPs was determined to be  $-0.48$  V vs. NHE, while the conduction band of the CdS NRs is  $-0.9$  V vs. NHE.<sup>[36]</sup> At pH 7, the  $\text{H}_2$  redox potential is  $-0.42$  V vs NHE. Because the conduction band of the  $\text{TiO}_2$  NPs is similar to the redox potential of  $\text{H}_2$ , it is difficult for  $\text{TiO}_2$  to photoreduce protons, thereby making the  $\text{TiO}_2$ -CdS system an ideal platform for studying Z-scheme photocatalysis.

Next, to generate  $\text{H}_2$  from the CdS NRs, Pt seeds were nucleated on the CdS through photodeposition.<sup>[40]</sup> TEM analysis showed that before and after platinum nucleation, the CdS nanocrystals retained their shape and size and that on average one Pt NP was bound per nanorod (Figure 1b). Next, ligand-exchange methods were developed to transfer the as-synthesized  $\text{TiO}_2$  and CdS NPs into aqueous environments. After trying various small molecules, we found that the most successful way to transfer the  $\text{TiO}_2$  NPs from toluene to water was to add a large excess of amine-(PEG)<sub>6</sub>-azide. For the Pt@CdS NRs, we used our previously developed method of small-molecule ligand exchange by mercaptoethanol or thioglycolic acid.<sup>[41]</sup>

Once the  $\text{TiO}_2$  and Pt@CdS NPs were transferred to the aqueous phase, DNA strands were conjugated to the NPs.

Previously developed methods were used to conjugate DNA strands to each Pt@CdS NR.<sup>[41]</sup> For the  $\text{TiO}_2$  NPs, click chemistry was implemented to form covalent bonds between the azide groups on the  $\text{TiO}_2$  and alkyne-terminated DNA (Supporting Information, Figure S3).<sup>[42]</sup> To qualitatively characterize DNA attachment, we reacted the DNA- $\text{TiO}_2$  with gold nanoparticles bound with complementary DNA. The AuNPs clearly associated with the  $\text{TiO}_2$  NPs through DNA hybridization (Supporting Information, Figure S4). The use of copper catalysts to conjugate the DNA to the  $\text{TiO}_2$  did not appear to affect the morphology or the absorption of the  $\text{TiO}_2$  NPs (Supporting Information, Figure S5).

Once the DNA strands were conjugated to both catalysts, we probed their ability to produce  $\text{H}_2$  at specific catalyst concentrations and compared these results to the azide-conjugated  $\text{TiO}_2$  and ME-Pt@CdS. First, the azide-terminated  $\text{TiO}_2$  NPs as expected showed almost no  $\text{H}_2$  production (Figure 2a). In contrast, 43 nm mercaptoethanol coated Pt@CdS NRs (ME-Pt@CdS) produced about 230 nmol of

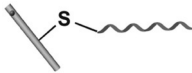
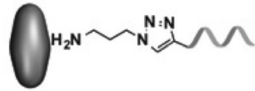
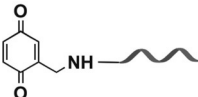
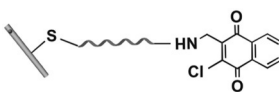
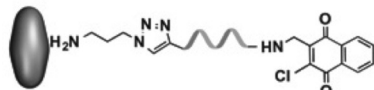


**Figure 2.** a)  $\text{H}_2$  production from Pt@CdS NRs conjugated with different amounts of DNA (molar ratio of CdS/DNA = 1:2, 1:10, 1:200), and amine-(PEG)<sub>4</sub>-azide coated  $\text{TiO}_2$ . Using molar ratios of CdS:DNA of 1:2 and 1:200 produced NRs attached with ca. 1.92 and ca. 189 DNA oligonucleotides, respectively, as determined by UV/Vis measurements. b)  $\text{H}_2$  production from Pt@CdS NRs with mercaptoethanol (ME) (■) and thioglycolic acid (TGA) (▲).

$\text{H}_2$ . Next, we measured  $\text{H}_2$  production from the Pt@CdS NRs conjugated with about 200 DNA strands per particle. As shown in Figure 2a, having a large number of DNA strands attached caused a significant decrease in  $\text{H}_2$  production as compared to the ME-Pt@CdS NRs. To determine if this effect was due to the presence of negatively charged groups at the photocatalyst surface, we also measured the amount of  $\text{H}_2$  produced from Pt@CdS NRs conjugated with thioglycolic acid (TGA). As shown in Figure 2b, a substantial decrease in  $\text{H}_2$  production was also observed from the negatively charged TGA-Pt@CdS as compared to the ME-Pt@CdS, indicating that the decrease in  $\text{H}_2$  production could be caused by the high negative charge of TGA or DNA. It is also possible in the case of DNA that a high coverage of oligonucleotides covering a particle surface could also hinder proton adsorption. However, decreasing the amount of DNA attached to the Pt@CdS NRs to about 2–5 oligonucleotides per particle led to an improvement in  $\text{H}_2$  production (Figure 2a) that gave results comparable to the ME-Pt@CdS NRs.

To assemble the  $\text{TiO}_2$ -Pt@CdS clusters through DNA interactions, the thiolated DNA (DNA-1) on the Pt@CdS was designed to contain two domains, one of which is comple-

**Table 1:** DNA design and sequence.

DNA name	DNA usage	DNA sequence
DNA 1		thiol-CATTACGGCTTTCCTATTA
DNA 2		alkyne-TAATAGGGAA
DNA 3		amine-TTTTTTAGCCGTAATG
DNA 4		thiol-CATTACGGCTTTCCTATTATTTTTT-amine
DNA 5		alkyne-TAATAGGGAA-amine

mentary to the DNA (DNA-2) on the  $\text{TiO}_2$ , with the other complementary to a third amine-terminated strand (DNA-3; Table 1). DNA-3 was used later to place electron mediators such as benzoquinone site-specifically in between the  $\text{TiO}_2$  and  $\text{Pt@CdS}$ . The DNA strands bridging the two photocatalysts were also designed to be 20 bases in length with a circa 40% G/C composition as this would yield good thermal stability in 100 mM NaCl and separate all the different components by 3–6 nm. After conjugating the DNA strands to the  $\text{TiO}_2$  and  $\text{Pt@CdS}$  using nanoparticle/DNA molar ratios of 1:5 and 1:2, respectively, thermal annealing was used to generate the  $\text{TiO}_2$ - $\text{Pt@CdS}$  clusters. TEM analysis of the DNA assembled catalysts showed the  $\text{TiO}_2$  and  $\text{Pt@CdS}$  nanoparticles to be well associated with each other with no large aggregates forming (Supporting Information, Figure S6).

Dynamic light scattering measurements also showed an average cluster size of about 247 nm (Supporting Information, Figure S7). Next, the  $\text{TiO}_2\text{-Pt@CdS}$  clusters were tested for  $\text{H}_2$  production. After photoirradiation under 1 sun for 2 h, the DNA assembled  $\text{TiO}_2\text{-Pt@CdS}$  nanoparticle clusters (Figure 3a) produced a significantly higher amount of  $\text{H}_2$  than the  $\text{TiO}_2$  or  $\text{Pt@CdS}$  NRs alone, with an overall gain of about 2.8 over  $\text{Pt@CdS}$  NR alone. Oxygen generated from the DNA linked  $\text{Pt@CdS-TiO}_2$  was also determined and showed approximately a 2:1  $\text{H}_2/\text{O}_2$  ratio as determined by GC (Supporting Information, Figure S8). It should also be noted that the catalyst amount used in this work (ca. 0.1 mg) was significantly less than that used in other reports.<sup>[1,15,16]</sup> To test the importance of DNA assembly,  $\text{H}_2$  production was measured from equimolar mixtures of mercaptoethanol-conjugated  $\text{Pt@CdS}$  NRs and amine-PEG-azide-coated  $\text{TiO}_2$  NPs. In contrast to the DNA-assembled  $\text{TiO}_2\text{-Pt@CdS}$  catalysts, a dispersed solution of the two photocatalysts showed no improvement over  $\text{Pt@CdS}$  itself (Figure 3a), illustrating that any  $\text{H}_2$  production enhancement was due solely to the DNA interaction. Furthermore, TEM analysis showed the DNA-linked  $\text{TiO}_2\text{-Pt@CdS}$  assemblies also

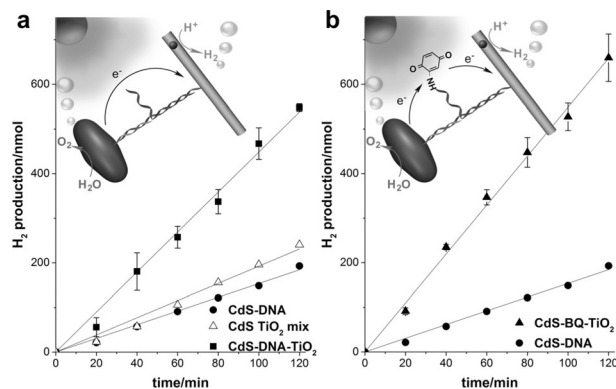


**Figure 3.** a)  $H_2$  production from DNA-conjugated Pt@CdS (●), DNA-linked  $TiO_2$ -Pt@CdS (■), and simple mixtures of unlinked Pt@CdS and  $TiO_2$  (△). b)  $H_2$  production from DNA-conjugated Pt@CdS (●) and from DNA-linked Pt@CdS–benzoquinone– $TiO_2$  system (▲).

proved to be stable during photoillumination (Supporting Information, Figure S9).

The next hypothesis tested was that placement of electron mediators specifically between the two photocatalysts would enhance H<sub>2</sub> production further by inhibiting back reactivity to facilitate charge separation. Benzoquinone (BQ) was chosen as a candidate because its reduction potential of 0.283 V vs. NHE at pH 7 lies between the conduction band (CB) of TiO<sub>2</sub> NP and the valence band (VB) of CdS NR. BQ was attached to DNA-3 strands through a Michael addition.<sup>[43,44]</sup> Mass spectrometric analysis confirmed the successful conjugation of BQ to the DNA-3 strand (Supporting Information, Figure S10). Cyclic voltammetry (CV) studies revealed that amine functionalization of BQ altered its reduction potential to circa 0.073 V vs NHE at pH 7 (Supporting Information, Figure S11), which is still in between the CB and VB of TiO<sub>2</sub> and CdS, respectively. We next hybridized equimolar amounts of the DNA-1-Pt@CdS, DNA-2-TiO<sub>2</sub>, and the DNA-3-BQ to make 43 nM concentrations of the Pt@CdS-BQ-TiO<sub>2</sub> and H<sub>2</sub> production was measured. As shown in Figure 3b, intercalat-



ing benzoquinone between the Pt@CdS and TiO<sub>2</sub> caused a further increase in H<sub>2</sub> production, with an overall 3.4-fold gain as compared to Pt@CdS itself and a 1.2-fold gain over the TiO<sub>2</sub>-Pt@CdS assemblies without BQ. It should also be noted that this process required a very low concentration (nM) of electron mediator. As a comparison, previously reported examples of non-assembled catalysts in solution required millimolar concentrations of redox mediators,<sup>[2]</sup> which can lead to deleterious effects such as competing oxidation–reduction reactions. Furthermore, when nanomolar concentrations of BQ were simply mixed with either the DNA assembled TiO<sub>2</sub>-Pt@CdS clusters or the Pt@CdS alone, no H<sub>2</sub> was produced due to BQ being competitively photoreduced in place of protons (Supporting Information, Figure S12). The solar-to-hydrogen (STH) energy conversion efficiency was also calculated. With 0.1 mg of Pt@CdS in solution, the STH values increased from 0.011 % with Pt@CdS to 0.031 % with TiO<sub>2</sub>-Pt@CdS to 0.037 % with the TiO<sub>2</sub>-BQ-Pt@CdS under one sun illumination at 97 mW cm<sup>-2</sup>.

Apart from utilizing a single electron mediator, the incorporation of a second mediator was tested. For this, 2,3-dichloro-1,4-naphthoquinone (DCNQ) was used, as its reduction potential of –0.077 V vs NHE is more positive than the CB of TiO<sub>2</sub> but more negative than the redox potential of BQ. In this case, the excited electrons are expected to travel from TiO<sub>2</sub> to DCNQ to BQ to Pt@CdS (Figure 4a). To achieve this, the DNA-1 strand was modified to include a thiol group at its 5' end and an amine at the 3' end (DNA-4), to place the DCNQ in close proximity to the TiO<sub>2</sub> NP (Figure 4b).<sup>[45]</sup> In testing the TiO<sub>2</sub>-DCNQ-BQ-Pt@CdS clusters however for catalysis, we found that less H<sub>2</sub> was produced than the Pt@CdS-BQ-TiO<sub>2</sub> system (Figure 4c). Although an additional redox mediator may facilitate the electron transfer, it is also possible that two intermediates may slow down the kinetics of the process owing to the additional redox step.

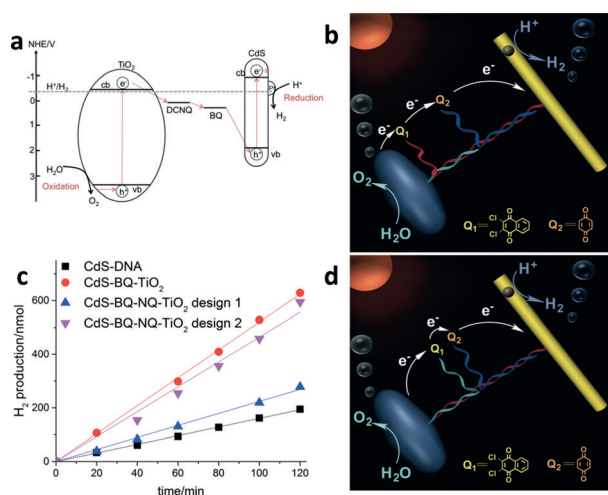


**Figure 4.** a) Energy band diagram of the Pt@CdS-BQ-DCNQ-TiO<sub>2</sub> system. b) H<sub>2</sub> production from Pt@CdS-BQ-DCNQ-TiO<sub>2</sub> design 1 system. c) H<sub>2</sub> production from Pt@CdS-BQ-DCNQ-TiO<sub>2</sub> assemblies versus Pt@CdS-BQ-TiO<sub>2</sub> (●) or Pt@CdS-DNA alone (■) design 1 (▲) design 2 (▼). d) H<sub>2</sub> production from CdS-BQ-DCNQ-TiO<sub>2</sub> design 2 system.

Because chronoamperometry studies however shown that the electron-transfer rates of BQ and DCNQ do not differ significantly from each other (Supporting Information, Figure S13), another more likely scenario is that the close proximity of the DCNQ to the TiO<sub>2</sub> leads to back reactivity, preventing electron mobility from DCNQ to BQ. To investigate this further, we modified DNA-2 to possess an alkyne at its 3' end and an amine at its 5' end (DNA-5; Table 1). This design would cause the DCNQ to be separated from the TiO<sub>2</sub> surface by about 3 nm but be immediately next to the BQ (Figure 4d). The TiO<sub>2</sub>-DNA-5-DCNQ were next hybridized with the DNA-1-Pt@CdS and DNA-3-BQ and tested for H<sub>2</sub> production. As shown in Figure 4c, while increasing the distance between the DCNQ and TiO<sub>2</sub> did increase the H<sub>2</sub> production from the first design of TiO<sub>2</sub>-DCNQ-BQ-Pt@CdS system (with DNA-4), the overall H<sub>2</sub> yield was comparable to the TiO<sub>2</sub>-BQ-Pt@CdS but not higher. Because the two quinones have similar energy levels and a similar electron-transfer rate, the electron transfer might not significantly change from the Pt@CdS-BQ-TiO<sub>2</sub> system, or the electron may even be prevented from transferring to the Pt@CdS by undergoing cyclic oxidation/reduction processes between the DCNQ and BQ. To cause an improvement in photocatalysis and H<sub>2</sub> production then, alternate quinones, increasing the distance between the mediators or using dynamic hybridization events need to be investigated in future studies.

In conclusion, a method was demonstrated for self-assembling different photocatalysts and electron mediators using DNA interactions for enhanced H<sub>2</sub> production. DNA was used to construct a well-organized Z-scheme photocatalytic system that could produce H<sub>2</sub> directly in water under solar illumination. The DNA assembled Pt@CdS and TiO<sub>2</sub> clusters showed a significant improvement in H<sub>2</sub> production compared to either single photocatalysts or unassembled, dispersed catalyst mixtures. Using DNA also enabled us to site specifically place electron mediators in between the TiO<sub>2</sub> and CdS and we found that while the use of benzoquinone alone improved H<sub>2</sub> production, utilizing an additional mediator did not improve catalysis. These results demonstrate that to increase the production of H<sub>2</sub> even more, both the redox potentials and spatial positioning of all the different Z-scheme components need to further optimized, and this will be studied in future work.

**Keywords:** DNA · electron mediators · hydrogen · photocatalysis · semiconductors

**How to cite:** *Angew. Chem. Int. Ed.* **2015**, *54*, 11490–11494  
*Angew. Chem.* **2015**, *127*, 11652–11656

- [1] Y. Sasaki, H. Nemoto, K. Saito, A. Kudo, *J. Phys. Chem. C* **2009**, *113*, 17536–17542.
- [2] Y. Sasaki, H. Kato, A. Kudo, *J. Am. Chem. Soc.* **2013**, *135*, 5441–5449.
- [3] R. Abe, K. Sayama, K. Domen, H. Arakawa, *Chem. Phys. Lett.* **2001**, *344*, 339–344.
- [4] H. Kato, M. Hori, R. Kenta, Y. Shimodaira, A. Kudo, *Chem. Lett.* **2004**, *33*, 1348–1349.
- [5] H. Tada, T. Mitsui, T. Kiyonaga, T. Akita, K. Tanaka, *Nat. Mater.* **2006**, *5*, 782–786.

- [6] J. Yu, S. Wang, J. Low, W. Xiao, *Phys. Chem. Chem. Phys.* **2013**, *15*, 16883–16890.
- [7] K. Maeda, *ACS Catal.* **2013**, *3*, 1486–1503.
- [8] Y. Tachibana, L. Vayssieres, J. R. Durrant, *Nat. Photonics* **2012**, *6*, 511–518.
- [9] H. Kato, Y. Sasaki, A. Iwase, A. Kudo, *Bull. Chem. Soc. Jpn.* **2007**, *80*, 2457–2464.
- [10] S. S. K. Ma, K. Maeda, T. Hisatomi, M. Tabata, A. Kudo, K. Domen, *Chem. Eur. J.* **2013**, *19*, 7480–7486.
- [11] T. Kothe, N. Plumeré, A. Badura, M. M. Nowaczyk, D. A. Guschin, M. Rogner, W. Schuhmann, *Angew. Chem. Int. Ed.* **2013**, *52*, 14233–14236; *Angew. Chem.* **2013**, *125*, 14483–14486.
- [12] D. J. Martin, P. J. T. Reardon, S. J. A. Moniz, J. Tang, *J. Am. Chem. Soc.* **2014**, *136*, 12568–12571.
- [13] G. Hitoki, T. Takata, J. N. Kondo, M. Hara, H. Kobayashi, K. Domen, *Chem. Commun.* **2002**, 1698–1699.
- [14] R. Abe, T. Takata, H. Sugihara, K. Domen, *Chem. Commun.* **2005**, 3829–3831.
- [15] K. Maeda, M. Higashi, D. Lu, R. Abe, K. Domen, *J. Am. Chem. Soc.* **2010**, *132*, 5858–5868.
- [16] H. J. Yun, H. Lee, N. D. Kim, D. M. Lee, S. Yu, J. Yi, *ACS Nano* **2011**, *5*, 4084–4090.
- [17] K. Sekizawa, K. Maeda, K. Domen, K. Koike, O. Ishitani, *J. Am. Chem. Soc.* **2013**, *135*, 4596–4599.
- [18] X. Wang, G. Liu, L. Wang, Z. Chen, G. Q. Lu, H. M. Cheng, *Adv. Energy Mater.* **2012**, *2*, 42–46.
- [19] S. Sato, T. Arai, T. Morikawa, K. Uemura, T. M. Suzuki, H. Tanaka, T. Kajino, *J. Am. Chem. Soc.* **2011**, *133*, 15240–15243.
- [20] Z. Liu, Z. G. Zhao, M. Miyauchi, *J. Phys. Chem. C* **2009**, *113*, 17132–17137.
- [21] A. Iwase, Y. H. Ng, Y. Ishiguro, A. Kudo, R. Amal, *J. Am. Chem. Soc.* **2011**, *133*, 11054–11057.
- [22] P. Zhou, J. Yu, M. Jaroniec, *Adv. Mater.* **2014**, *26*, 4920–4935.
- [23] C. Li, J. Yuan, B. Han, L. Jiang, W. Shangguan, *Int. J. Hydrogen Energy* **2010**, *35*, 7073–7079.
- [24] X. Liu, A. Niazov-Elkan, F. Wang, I. Willner, *Nano Lett.* **2013**, *13*, 219–225.
- [25] D.-K. Lim, K.-S. Jeon, H. M. Kim, J.-M. Nam, Y. D. Suh, *Nat. Mater.* **2010**, *9*, 60–67.
- [26] W. Yan, L. Xu, C. Xu, W. Ma, H. Kuang, L. Wang, N. A. Kotov, *J. Am. Chem. Soc.* **2012**, *134*, 15114–15121.
- [27] L. Xu, H. Kuang, C. Xu, W. Ma, L. Wang, N. A. Kotov, *J. Am. Chem. Soc.* **2012**, *134*, 1699–1709.
- [28] R. Schreiber, J. Do, E.-M. Roller, T. Zhang, V. J. Schuller, P. C. Cickels, J. Feldmann, T. Liedl, *Nat. Nanotechnol.* **2014**, *9*, 74–76.
- [29] G. P. Acuna, M. Bucher, I. H. Stein, C. Steinhauer, A. Kuzyk, P. Holzmeister, R. Schreiber, A. Moroz, F. D. Stefani, T. Liedl, F. C. Simmel, P. Tinnefeld, *ACS Nano* **2012**, *6*, 3189–3195.
- [30] H. Yan, S. H. Park, G. Finkelstein, J. H. Reif, *Science* **2003**, *301*, 1882–1884.
- [31] J. Sharma, Y. Ke, C. Lin, R. Chhabra, Q. Wang, J. Nangreave, Y. Liu, H. Yan, *Angew. Chem. Int. Ed.* **2008**, *47*, 5157–5159; *Angew. Chem.* **2008**, *120*, 5235–5237.
- [32] J. Liu, Y. Lu, *J. Am. Chem. Soc.* **2003**, *125*, 6642–6643.
- [33] R. Tel-Vered, O. Yehezkeili, H. B. Yildiz, O. I. Wilner, I. Willner, *Angew. Chem. Int. Ed.* **2008**, *47*, 8272–8276; *Angew. Chem.* **2008**, *120*, 8396–8400.
- [34] W. Sun, E. Boulais, Y. Hakobyan, W. L. Wang, A. Guan, M. Bathe, P. Yin, *Science* **2014**, *346*, 1258361.
- [35] H. T. Maune, S.-p. Han, R. D. Barish, M. Bockrath, W. A. Goddard III, P. W. K. Rothmund, E. Winfree, *Nat. Nanotechnol.* **2010**, *5*, 61–66.
- [36] R. Gill, F. Patolsky, E. Katz, I. Willner, *Angew. Chem. Int. Ed.* **2005**, *44*, 4554–4557; *Angew. Chem.* **2005**, *117*, 4630–4633.
- [37] C.-T. Dinh, T.-D. Nguyen, F. Kleitz, T.-O. Do, *ACS Nano* **2009**, *3*, 3737–3743.
- [38] R. D. Robinson, B. Sadtler, D. O. Demchenko, C. K. Erdonmez, L.-W. Wang, A. P. Alivisatos, *Science* **2007**, *317*, 355–358.
- [39] S. K. Haram, B. M. Quinn, A. J. Bard, *J. Am. Chem. Soc.* **2001**, *123*, 8860–8861.
- [40] G. Dukovic, M. G. Merkle, J. H. Nelson, S. M. Hughes, A. P. Alivisatos, *Adv. Mater.* **2008**, *20*, 4306–4311.
- [41] H. Noh, S. M. Goodman, P. Mohan, A. P. Goodwin, P. Nagpal, J. N. Cha, *RSC Adv.* **2014**, *4*, 8064.
- [42] V. Hong, S. I. Presolki, C. Ma, M. G. Finn, *Angew. Chem. Int. Ed.* **2009**, *48*, 9879–9883; *Angew. Chem.* **2009**, *121*, 10063–10067.
- [43] J. S. Yadav, B. V. S. Reddy, T. Swamy, K. S. Shankar, *Monatsh. Chem.* **2008**, *139*, 1317–1320.
- [44] E. Katz, H.-L. Schmidt, *J. Electroanal. Chem.* **1993**, *360*, 337–342.
- [45] V. K. Tandon, H. K. Maurya, *Tetrahedron Lett.* **2009**, *50*, 5896–5902.

Received: May 6, 2015

Revised: May 29, 2015

Published online: July 1, 2015